

# Stable Low-Repetition-Rate Time-Lens Picosecond Seed Source

C. Dorrer and R. J. Brown

**Abstract**—The design and performance of a sub-10-picosecond source based on temporal focusing implemented with a lithium niobate phase modulator and grating compressor are presented. The source is optimized taking into account spectral gain narrowing in subsequent amplifiers. It advantageously delivers low-repetition-rate pulses with tunable pulse duration, and its short-term jitter and long-term drift over extended periods of time are of the order of a few picoseconds.

**Index Terms**—Chromatic dispersion, optical pulse generation, phase modulation, pulse compression methods.

## I. INTRODUCTION

MODE-LOCKING makes it possible to generate short optical pulses with durations down to a few optical cycles, but alternatives have been demonstrated [1–5]. Their potential advantages include repetition rate tunability, in the absence of round-trip time constraints from an optical cavity; simple wavelength tunability using a monochromatic seed source; and adjustability of energy and duration in the absence of peak-power constraints for nonlinearity-based mode locking.

We demonstrate a time-lens optical source with emphasis on pulse-duration tunability and long-term temporal stability because of the intended application as a seed source for a frequency-quadrupled laser synchronized to a high-energy laser system [6].

## II. DESIGN

### A. Principle

The source is based on the concept of spatiotemporal duality [7,8]. In the spatial domain [Fig. 1(a)], a lens of focal length  $f$  imparts a quadratic spatial phase on the transmitted wave. Diffraction in the Fresnel approximation induces a quadratic phase in the wave-vector domain and focuses the wave at a distance approximately equal to  $f$ . The time-frequency equivalent of spatial focusing combines a quadratic temporal phase, e.g., from a phase modulator, and a quadratic spectral phase, e.g., from a grating compressor [Fig. 1(b)]. A Fourier transform-limited Gaussian input pulse with full width at half maximum (FWHM)  $\Delta t_0$  propagating in a temporal lens with coefficient  $\psi_2$  and a compressor inducing a quadratic spectral phase  $\varphi_2=1/[\psi_2(1+\rho)]$  leads to a Fourier-transform-limited

Gaussian pulse with FWHM equal to  $\Delta t_0/\sqrt{(1+1/\rho)}$ , where  $\rho = \left[4\ln(2)/(\psi_2\Delta t_0^2)\right]^2$ . The output pulse is significantly compressed when  $\rho = 1$ , i.e.,  $\psi_2 = 1/\Delta t_0^2$ , in which case  $\varphi_2\psi_2 \sim 1$ . This regime is less demanding than temporal imaging [8], which requires the addition of dispersion before the time lens, in turn requiring more components and a larger aperture for the time lens.

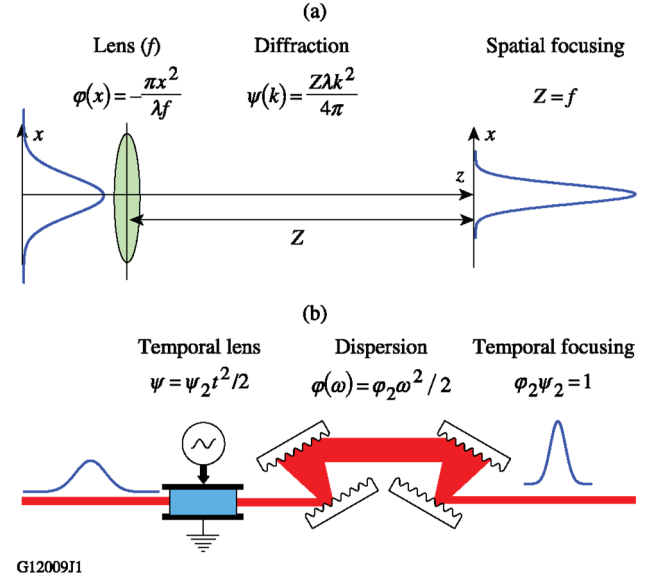


Fig. 1. Principle of (a) spatial focusing by a lens and diffraction and (b) temporal focusing by a time lens and chromatic dispersion.

### B. Simulations

Operation parameters have been identified by simulations. The phase of the input pulse with FWHM  $\Delta t_0 = 50$  ps is temporally modulated by a sinusoidal drive at 8 GHz, which is mostly quadratic, with either a positive or negative coefficient, over the temporal support of the pulse for adequate timing. The pulse then propagates in a grating compressor, which can introduce large amounts of chromatic dispersion with higher stability than optical fibers. Because the compressor has  $\varphi_2 < 0$ , the temporal-phase modulation must have  $\psi_2 < 0$ , i.e., the pulse is synchronized with a maximum of the sinusoidal phase. We consider a compressor with commercially available 1700 l/mm

This material is based upon work supported by the Department of Energy National Nuclear Security Administration under Award Number DE-NA0001944, the University of Rochester, and the New York State Energy Research and Development Authority.

C. Dorrer and R. J. Brown are with the Laboratory for Laser Energetics, University of Rochester, Rochester, NY 14623-1299 USA (email: [cdorrer@lle.rochester.edu](mailto:cdorrer@lle.rochester.edu); [rbro@lle.rochester.edu](mailto:rbro@lle.rochester.edu)).

transmission gratings operating at the Littrow angle ( $63.5^\circ$  incident and diffracted angles), with distance  $L$  between the first and second gratings at the 1053-nm central wavelength.

Fig. 2(a) displays the output FWHM as a function of the phase modulation index  $m$  and distance  $L$ . For temporal focusing, the optimal value of  $L$  leading to the shortest pulse is expected to be inversely proportional to  $m$ , but different optimal combinations of  $m$  and  $L$  are observed because the phase modulation is not purely quadratic over the temporal support of the input pulse. The resulting non-Gaussian optical spectrum leads to discontinuities of the output FWHM at some locations of the parameter space. Larger phase modulations corresponding to higher microwave power in the phase modulator yield shorter compressed pulses and require a smaller compressor.

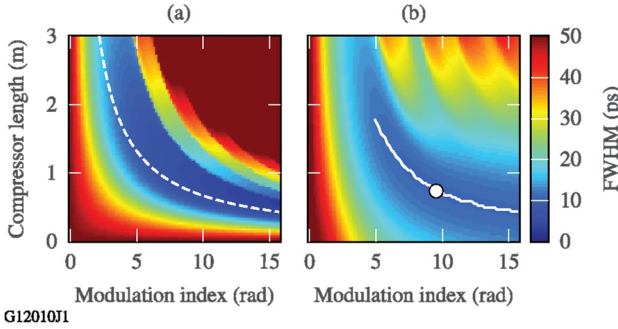


Fig. 2. Simulated FWHM (a) after the compressor and (b) after spectral gain narrowing, as a function of phase-modulation index and compressor length. The color bar has been adjusted to clamp values larger than the input FWHM. The dashed white line in (a) indicates the locus of points such as  $\varphi_2 \psi_2 = 1$ . The white line on (b) indicates FWHM within 10% of the Fourier transform limit.

Our application requires further amplification, which leads to spectral narrowing. Gain narrowing was modeled as a Gaussian transfer function with FWHM = 0.15 nm, which is similar to the commonly measured spectrum of the laser fluorescence generated by a Nd:YLF regenerative amplifier, but the general conclusions derived from simulations do not depend significantly on these parameters. Figure 2(b) displays the FWHM after spectral gain narrowing. The white line indicates the locus of the modulation index and corresponding optimal compressor length leading to FWHM within 10% of the Fourier transform-limited duration for that amplifier. Because of spectral narrowing, higher modulation indices do not yield shorter pulse durations. Instead, they lead to poorer overlap of the seed's spectrum with the amplifier's spectral gain. These findings are quantified in Fig. 3. The goal of a modulation index equal to  $3\pi$  was identified [solid circles in Figs. 2(b), 3(a), and 3(b)], based on the trade-offs between microwave power, compressor length, and seeding efficiency.

### III. EXPERIMENTAL RESULTS

#### A. Design

The source's layout is displayed in Fig. 4. Synchronization to a reference clock at  $f_{\text{ref}} = 75.997870$  MHz and trigger signals is required to generate pulses synchronized with other sources in the laboratory. A pulse generator driving two successive

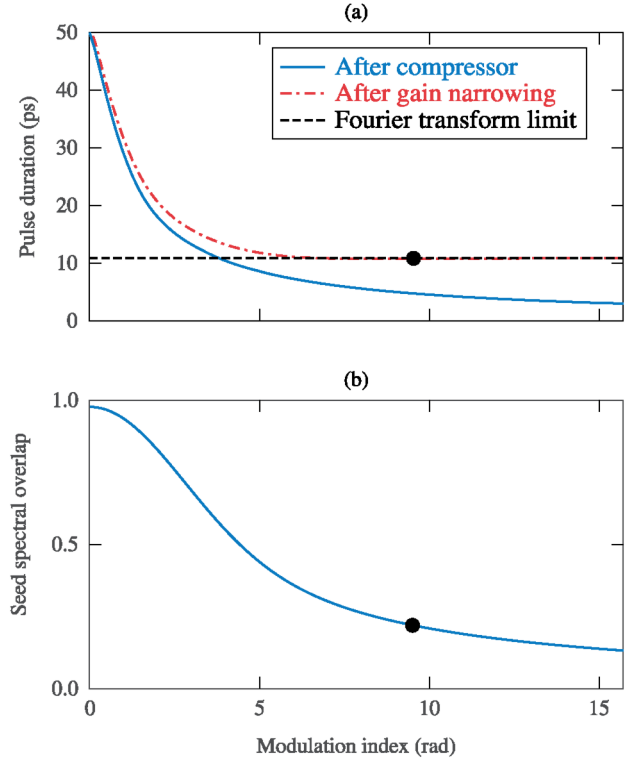


Fig. 3. (a) FWHM after the compressor (blue line) and after gain narrowing (red line), compared to the Fourier transform-limited FWHM (dashed line). (b) Spectral overlap of the seed spectrum with the Gaussian 0.15-nm gain function of the amplifier.

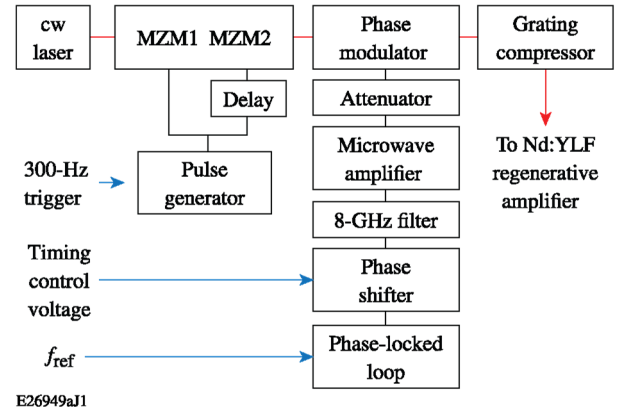


Fig. 4. Source's layout. Two fiber amplifiers and one acousto-optic modulator, which are not fundamental to the source's operation, are not displayed. MZM: Mach-Zehnder modulator.

Mach-Zehnder modulators (MZM's) biased at extinction carves an  $\sim 50$ -ps pulse at 1053 nm. A phase-locked loop generates the phase-modulation frequency  $f \sim 8$  GHz as the 105th multiple of  $f_{\text{ref}}$ . The high-frequency signal is then timed via a voltage-controlled phase shifter and amplified by a 33-dBm amplifier, leading to a modulation index as high as 13.5 rad. The compressor has a single 1700-l/mm transmission diffraction grating with roof mirrors in the horizontal and vertical directions to allow for four passes on the grating. The source operates at 300 Hz (one of the standard laboratory rates), but operation at any other rate synchronized with  $f_{\text{ref}}$  is possible. Energies of the order of 20 pJ, sufficient to seed the Nd:YLF

regenerative amplifier, were obtained, while energies of the order of 0.5 mJ were obtained after the amplifier.

### B. Temporal Recompression

The source has been temporally characterized using a high-bandwidth photodetector and a 70-GHz real-time oscilloscope. The resulting impulse response, determined by measuring a subpicosecond pulse from a mode-locked laser, has a FWHM equal to 13.5 ps. This calibrated value was directly used to deconvolve the measured pulse durations. Intensity autocorrelations measured after the regenerative amplifier did not reliably assess the pulse duration because the autocorrelation deconvolution factor depends strongly on the pulse's exact shape, particularly in the low-intensity regions.

The measured durations are 46 ps after the Mach-Zehnder modulators and  $15.5 \pm 0.8$  ps after recompression [Fig. 5(a)]. After amplification in the Nd:YLF regenerative amplifier, the measured FWHM is  $16.5 \pm 0.6$  ps. The  $\pm$  interval in those determinations has a width equal to twice the standard deviation determined over at least 24 h of operation, which was determined using an assumed stable mode-locked laser to be dominated by measurement noise. The pulse duration at the regenerative-amplifier output is similar to that obtained by seeding with a 7-ps pulse from a mode-locked laser ( $16.5 \pm 0.5$  ps). The deconvolved pulse durations are 7.6 ps and 9.6 ps after the compressor and after the regenerative amplifier, respectively.

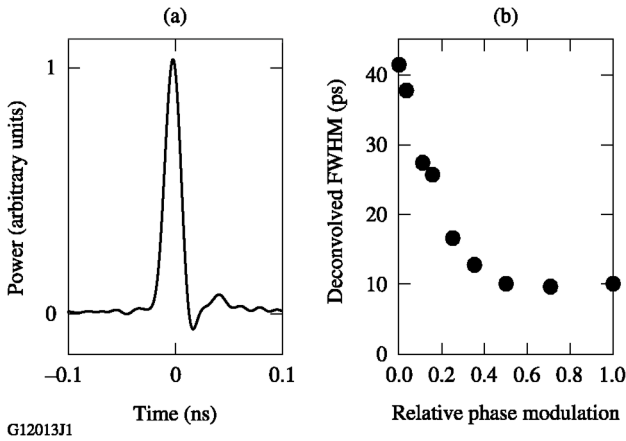


Fig. 5. (a) Measured pulse after temporal focusing. (b) Deconvolved FWHM as a function of the phase modulation relative to the largest observed modulation.

The output-pulse duration was tuned by decreasing the phase-modulation index while keeping the compressor length fixed. Discrete microwave attenuators were inserted before the phase modulator to address the full FWHM range from  $\sim 45$  ps to  $\sim 10$  ps [Fig. 5(b)], but a remotely controllable digital attenuator before the microwave amplifier will be used in the deployed system. Pulses longer than 45 ps can be obtained simply by increasing the duration of the gate pulse provided by the pulse generator without phase modulation.

### C. Timing Stability

Short-term jitter of the low-repetition-rate source was measured relative to the stable timing reference provided by a mode-locked laser synchronized to  $f_{\text{ref}}$ . Pulses from the two

sources are combined with a fiber coupler and measured on the same oscilloscope channel. The relative delay between the two pulses is extracted via Fourier filtering, independently of the scope's trigger jitter [9], leading to a determination of 3.4-ps peak-to-valley and 1.8-ps rms jitter over 100 acquisitions taken over  $\sim 5$  s [Fig. 6(a)]. These values include the measurement noise (1.8-ps peak-to-valley and 0.4-ps rms) determined by applying the same procedure to two successive pulses from the mode-locked laser, which are assumed to have negligible relative jitter. The long-term drift was measured by quantifying the source's output timing every 5 min relative to the time base of the oscilloscope triggered by a high-precision trigger synchronized to  $f_{\text{ref}}$ . To reduce the measurement noise, the timing was determined as the average over 100 oscilloscope acquisitions performed over 5 s. Fig. 6(b) shows that the drift over more than 50 h is lower than a few picoseconds. The measured short-term jitter and long-term drift are acceptable considering the pulse duration and application. As a comparison, the stability of two commercial mode-locked Nd:glass oscillators actively synchronized to  $f_{\text{ref}}$  and delivering either a 7-ps pulse or a 200-fs pulse was determined under the same environmental conditions (Fig. 7). The significantly larger variations are attributed to drifts in the synchronization units or in the optical cavities.

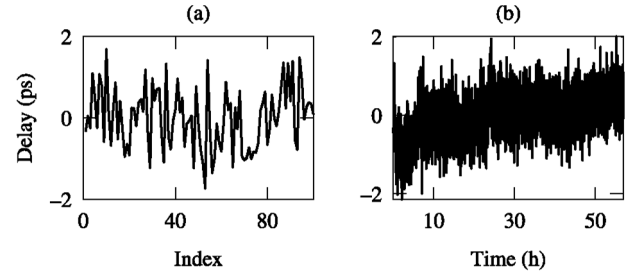


Fig. 6. Timing of time-lens source relative to (a) a mode-locked laser over 5 s and (b) the time base of the oscilloscope over 55 h.

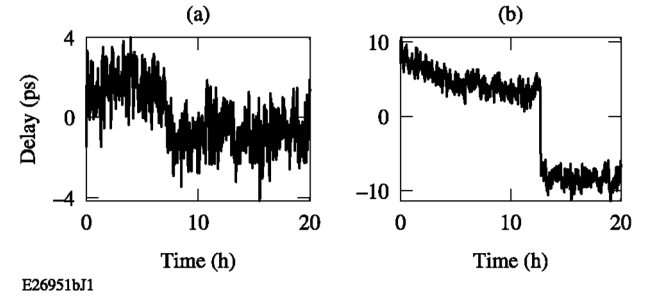


Fig. 7. [(a),(b)] Timing of two different commercial mode-locked lasers synchronized to  $f_{\text{ref}}$ .

### D. Low-Bandwidth Optimization

We have investigated a performance metric obtainable via low-bandwidth detectors after an intensity-dependent process, similar to adaptive pulse compression [10], to optimize the relative timing between optical pulse and phase modulation without high-bandwidth photodetection. A fraction of the regenerative-amplifier output generates a reference energy signal  $E_{1\omega}$  at the fundamental frequency and produces an up-converted pulse by second-harmonic generation in a phase-matched nonlinear crystal, resulting in the energy signal  $E_{2\omega}$ .

$E_{1\omega}$  and  $E_{2\omega}$  can be obtained, for example, using cameras or energy meters. The pulse-quality metric  $\eta = E_{2\omega}/(E_{1\omega})^2$  increases for shorter pulses and reduced pre- and post pulses.

Fig. 8(a) shows the good agreement between the metric determined experimentally and numerically calculated using the measured pulse shapes, identifying the same optimal phase-shifter control voltage (1.1 V). Convolution with the photodetection impulse response results in smaller pulse-duration variations than in the actual pulse and lower variations of the calculated metric compared to the measured metric. Fig. 8(b) shows pulses measured at two non-optimal control voltages (0.9 V and 1.3 V), with higher pre-/postpulses than at the optimal control voltage (1.1 V).

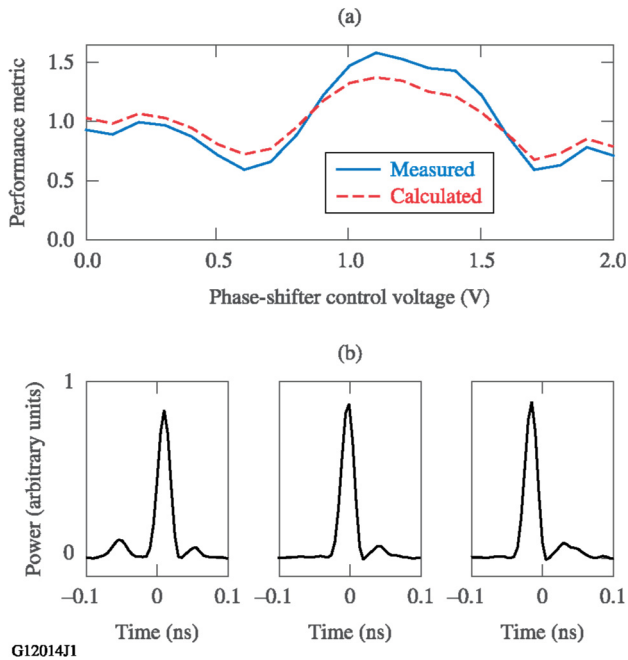


Fig. 8. (a) Measured (blue curve) and calculated (red curve) performance metric versus phase-shifter control voltage. The 2-V range approximately corresponds to linear scanning of the relative delay over the 125-ps ( $= 1/8$ -GHz) period. (b) Measured pulse shapes at 0.9 V, 1.1 V, and 1.3 V (from left to right). Photodiode ringing leads to a postpulse  $\sim 40$  ps after the main pulse.

#### IV. CONCLUSIONS

We have presented the design and performance of a low-repetition-rate sub-10-ps time-lens-based source with precise short-term and long-term synchronization to a reference frequency. The non-quadratic time lens and spectral gain narrowing in a subsequent amplifier have been taken into account. The source, which performs comparably to or better than several commercial laser systems, but with the advantage of pulse-duration tunability, will provide seed pulses for a 20-mJ laser system at 263 nm [6]. Other potential applications include generating tunable seed pulses for pulse stacking and picket-fence pulse shaping [11,12].

#### ACKNOWLEDGMENT

This report was prepared as an account of work sponsored by an agency of the U.S. Government. Neither the U.S. Government nor any agency thereof, nor any of their

employees, makes any warranty, express or implied, or assumes any legal liability or responsibility for the accuracy, completeness, or usefulness of any information, apparatus, product, or process disclosed, or represents that its use would not infringe privately owned rights. Reference herein to any specific commercial product, process, or service by trade name, trademark, manufacturer, or otherwise does not necessarily constitute or imply its endorsement, recommendation, or favoring by the U.S. Government or any agency thereof. The views and opinions of authors expressed herein do not necessarily state or reflect those of the U.S. Government or any agency thereof.

#### REFERENCES

- [1] B. H. Kolner, "Active pulse compression using an integrated electro-optic phase modulator," *Appl. Phys. Lett.*, vol. 52, no. 14, pp. 1122–1124, 1988.
- [2] J. van Howe, J. H. Lee, and C. Xu, "Generation of 3.5 nJ femtosecond pulses from a continuous-wave laser without mode locking," *Opt. Lett.*, vol. 32, no. 11, pp. 1408–1410, 2007.
- [3] M. A. Prantil, E. Cormier, J. W. Dawson, D. J. Gibson, M. J. Messerly, and C. P. J. Barty, "Widely tunable 11 GHz femtosecond fiber laser based on a nonmode-locked source," *Opt. Lett.*, vol. 38, no. 17, pp. 3216–3218, 2013.
- [4] A. Aubourg, J. Lhermite, S. Hocquet, E. Cormier, and G. Santarelli, "Generation of picosecond laser pulses at 1030 nm with gigahertz range continuously tunable repetition rate," *Opt. Lett.*, vol. 40, no. 23, pp. 5610–5613, 2015.
- [5] W. Fu, L. G. Wright, and F. W. Wise, "High-power femtosecond pulses without a modelocked laser," *Optica*, vol. 4, no. 7, pp. 831–834, 2017.
- [6] D. H. Froula, R. Boni, M. Bedzyk, R. S. Craxton, F. Ehrne, S. Ivancic, R. Jungquist, M. J. Shoup, W. Theobald, D. Weiner, N. L. Kugland, and M. C. Rushford, "Optical diagnostic suite (Schlieren, interferometry, and grid image refractometry) on OMEGA EP using a 10-ps, 263-nm probe beam," *Rev. Sci. Instrum.*, vol. 83, no. 10, p. 10E523, 2012.
- [7] P. Tournois, "Analogie optique de la compression d'impulsion," *C. R. Acad. Sci.*, vol. 258, no. 15, pp. 3839–3842, 1964.
- [8] B. H. Kolner, "Space-time duality and the theory of temporal imaging," *IEEE J. Quantum Electron.*, vol. 30, no. 8, pp. 1951–1963, 1994.
- [9] C. Dorrer, W. A. Bittle, R. Cuffney, M. Spilatro, E. M. Hill, T. Z. Kosc, J. H. Kelly, and J. D. Zuegel, "Characterization and optimization of an eight-channel time-multiplexed pulse-shaping system," *J. Lightwave Technol.*, vol. 35, no. 2, pp. 173–185, 2017.
- [10] D. Yelin, D. Meshulach, and Y. Silberberg, "Adaptive femtosecond pulse compression," *Opt. Lett.*, vol. 22, no. 23, pp. 1793–1795, 1997.
- [11] J. E. Rothenberg, "Ultrafast picket fence pulse trains to enhance frequency conversion of shaped inertial confinement fusion laser pulses," *Appl. Opt.*, vol. 39, no. 36, pp. 6931–6938, 2000.
- [12] I. Will and G. Klemz, "Generation of flat-top picosecond pulses by coherent pulse stacking in a multicrystal birefringent filter," *Opt. Express*, vol. 16, no. 19, pp. 14922–14937, 2008.